Pareto fronts reveal constraints on the evolution of niche-determining traits in phytoplankton

Jason R. Laurich[1], Anita Narwani[2], & Joey R. Bernhardt[1]

[1]Department of Integrative Biology, University of Guelph, Guelph, ON, Canada

[2]Department of Aquatic Ecology, Swiss Federal Institute of Aquatic Science and Technology (Eawag), Dübendorf, Switzerland

*Corresponding author: Jason R. Laurich

Email: jlaurich@uoguelph.ca

Author Contributions:

Conceptualization: J.R.L., A.N., J.R.B. Data curation: J.R.L., A.N., J.R.B. Formal analysis: J.R.L. Funding acquisition: A.N., J.B. Investigation: J.R.L., J.B. Methodology: J.R.L., A.N., J.B. Project administration: J.R.L., A.N., J.R.B. Resources: A.N., J.R.B. Software: J.R.L. Supervision: J.R.B. Validation: J.R.L., J.B. Visualization: J.R.L. Writing—original draft: J.R.L. Writing—review & editing: J.R.L., A.N., J.R.B.

Competing Interest Statement: The authors have no competing interests to declare.

Keywords: Pareto fronts, evolutionary constraint, trade-offs, ecological limits, phytoplankton.

Abstract

Trade-offs are central to biodiversity because they prevent the emergence of dominant phenotypes by limiting the simultaneous optimization of multiple fitness components. Yet trade-offs are often difficult to detect empirically when variation in overall performance produces positive correlations that mask underlying constraints. Here we use Pareto fronts—boundaries that capture optimal trade-off solutions—to test for evolutionary constraints on niche-determining traits in phytoplankton, including minimum nutrient requirements, thermal breadth, salt tolerance, and population growth rates. Using experimentally evolved *Chlamydomonas reinhardtii* populations subjected to nutrient and salt stress, we detected widespread Pareto fronts limiting the joint optimization of growth rate and niche-determining traits, thereby restricting the emergence of multivariate stress tolerance. Importantly, Pareto fronts revealed trade-offs even when underlying trait correlations were positive. We found that the structure of trait covariation behind Pareto fronts strongly predicted evolutionary outcomes: populations moved toward Pareto-optimal phenotypes primarily when trait correlations were neutral or positive, whereas negative trait correlations were associated with limited evolutionary optimization. Extending this framework across phytoplankton diversity, we compiled niche-determining traits for 299 phytoplankton taxa. At a macroevolutionary scale, we detected significant Pareto fronts constraining the evolution of niche-determining traits in phytoplankton. These fronts, however, did not always recapitulate the structure of trade-offs evident among *C. reinhardtii* populations, suggesting that forces that dictate microevolutionary outcomes, such as genetic correlations, can be resolved across macroevolutionary time. Together, our results highlight that evolutionary trajectories may differ across scales, but that fundamental limits on multivariate trait optimization persist across phytoplankton.

Significance Statement

Trade-offs among biological traits are central to evolutionary theory but often prove difficult to detect empirically. Here, we apply Pareto fronts—a framework borrowed from economics and

engineering—to detect and reveal trade-offs among key niche-determining traits in phytoplankton. By combining experimental evolution in the laboratory with a synthesis of ecological traits across 299 taxa, we demonstrate widespread limits on the simultaneous optimization of growth rate, nutrient competition, salt tolerance, and thermal breadth. Importantly, Pareto fronts reveal trade-offs even when conventional correlation-based approaches fail, uncovering evolutionary constraints that remain hidden in trait correlations. These results show that trade-offs shape phenotypic variation across both micro- and macroevolutionary scales and impose fundamental limits on phytoplankton responses to multiple environmental stressors.

Main Text

Introduction

Since Darwin first remarked on his “tangled bank” of biodiversity (1), evolutionary ecologists have grappled with a central problem in ecology and evolution: identifying the forces that shape—and constrain—the patterns of trait variation that constitute Earth’s biodiversity (2). Among the most important of these forces are fundamental trade-offs between fitness-determining traits (1, 3–5). By preventing the simultaneous optimization of multiple traits, trade-offs have long been viewed as primary obstacles to the emergence of “Darwinian demons”—hypothetical genotypes capable of maximizing all aspects of fitness (6, 7). Variation in how organisms navigate these trade-offs is widely invoked to explain ecological specialization, niche differentiation, and the coexistence of competing species (8–11).

Beyond shaping patterns of biological variation, trade-offs are central to predicting evolutionary responses to environmental change. Natural selection acts on organisms through inherently multivariate selective landscapes, operating on interacting traits that together determine fitness (12). Consequently, evolutionary responses depend not only on the direction and strength of selection but also on the structure of trade-offs that constrain coordinated trait evolution (13). The consequences of such trade-offs may be especially acute under anthropogenic change, as human activities increasingly expose organisms to multiple, co-occurring stressors including warming, salinization, pollution, and altered nutrient regimes (14–17).

Primary producers such as phytoplankton, which underpin aquatic food webs and drive global biogeochemical cycles (18, 19), face complex multivariate selection acting on key niche-determining traits. Traits including growth rate, minimum nutrient requirements (R^*), thermal breadth, and salt tolerance play central roles in defining phytoplankton niches and species persistence under environmental change and are hypothesized to be linked by trade-offs (11). Classic examples include trade-offs within individual niche axes such as gleaner–opportunist (20–23), tolerance–growth (24, 25), and generalist–specialist (26) strategies. Trade-offs may also arise across niche axes—for example between performance under low light and low nutrient conditions—depending on whether traits share physiological pathways or compete for limited energetic or cellular resources (27–30). Where present, such trade-offs should exert powerful constraints on evolutionary responses to environmental change. Yet despite their central role in ecological and evolutionary theory, the extent to which trade-offs shape phenotypic variation in natural systems remains uncertain, and clear empirical evidence for them is often elusive (3, 5, 31).

Trade-offs are frequently obscured in empirical data, where traits presumed to trade off often exhibit positive correlations instead (3, 5, 31, 32). This pattern can arise because individuals and species vary widely in overall performance due to physiological, genetic, and environmental differences (33). When variation in organismal quality is large, high-performing individuals may perform well across multiple tasks simultaneously, masking underlying constraints (Fig. 1A). Nevertheless, theory dictates that no genotype can simultaneously maximize all aspects of fitness (6, 34, 35).

Trade-offs can therefore become apparent among relatively optimized phenotypes (3, 36–38), where constraints emerge as Pareto fronts that represent the set of optimal solutions to trade-offs and thus delineate limits to multivariate trait optimization (35, 39, Fig. 1A). For genotypes located on or near a Pareto front, simultaneous improvement in multiple traits is expected to be exceedingly unlikely (39, 40). Nonetheless, sufficiently strong or novel selection pressures may occasionally shift the location of a Pareto front by favoring mutations that improve performance across multiple traits simultaneously (Fig. 1B), particularly when constraints imposed by other aspects of organismal biology—such as cell size, defense, or additional niche axes in phytoplankton (23, 27, 29, 41)—are relaxed.

Across macroevolutionary timescales, the cumulative effects of selection acting on many traits across diverse organisms and environments are expected to reveal fundamental trade-offs that have yet to be resolved (5). When selection strongly favours optimization along a particular pair of traits, species are predicted to sort along Pareto fronts, producing negative correlations near the upper bounds of performance (42–46) (Fig. 1C). In contrast, when interspecific variation reflects broad patterns of specialization and divergence in ecological niches and life history strategies, multivariate selection on suites of traits can produce triangular constraint envelopes balancing trade-offs in performance across multiple axes (10, 24, 27, 35, Fig. 1D). Because genetic constraints are less relevant over long evolutionary timescales (47–50), such macroevolutionary patterns may provide clearer signatures of biophysical or physiological trade-offs than those observed among populations or genotypes (3, 31). Consequently, the boundaries of phenotypic space occupied by species are expected to reflect fundamental physiological or ecological limits to trait optimization rather than transient genetic constraints. As a result, the shape of phenotypic variation across species is expected to represent not merely the outcome of historical contingency, but the long-term imprint of intractable trade-offs that constrain evolutionary possibilities.

In this study, we combined experimental evolution and comparative data synthesis to examine how Pareto fronts shape patterns of phenotypic variation and constraint across micro- and macroevolutionary scales in phytoplankton. Using 37 experimentally evolved populations of *Chlamydomonas reinhardtii*, we first tested (1) whether Pareto fronts constrain relationships between growth and key niche-determining traits within and across environmental gradients, and (2) under what conditions experimental evolution drives populations toward Pareto-optimal trait combinations. We then extended this framework to a synthesis of niche-determining traits across 299 phytoplankton taxa to test (3) whether the signatures of Pareto constraint observed in experimentally evolved *C. reinhardtii* populations are reflected in macroevolutionary patterns of trait variation. Focusing on trade-offs involving nutrient competition, salt tolerance, and thermal performance—traits central to phytoplankton niches under contemporary environmental change—we evaluate how constraints on multivariate trait optimization emerge and persist across evolutionary scales.

Results

Trade-offs between growth and niche-determining traits in *Chlamydomonas reinhardtii*. To investigate trade-offs between maximum growth rates and key niche-determining traits, we experimentally evolved five ancestral populations of *Chlamydomonas reinhardtii* under salt stress (S), light (I), and nutrient limitation (N- nitrogen, P- phosphorus, *SI Methods*). After approximately 285 generations, we assayed ancestral and descendant populations across gradients of light, nitrogen, phosphorus, salt, and temperature to estimate maximum growth rates (μ_{max}), thermal breadth (T_{br}), salt tolerance (c), and competitive abilities for limiting resources (Fig. S1). We defined

competitive ability as $1/R^*$ (21), the inverse of the minimum resource level required for population persistence (R^*).

We focused first on trade-offs between *C. reinhardtii* growth rates and niche-determining traits within individual niche axes. Here, classical ecological trade-offs such as gleaner-opportunist, generalist-specialist, and growth-tolerance trade-offs are expected to arise directly from physiological constraints that limit simultaneous optimization along a single dimension of environmental variation—for example when adaptations that improve growth under low resource availability reduce maximum growth rate when that resource is replete (20, 21, 24–26). To identify trade-offs among phenotypes approaching optimal trait combinations, we characterized putative Pareto fronts using a modified convex hull algorithm and fit shape-constrained additive models to Pareto-optimal phenotypes. We also fit median (50th) quantile regressions to assess the strength and direction of trait correlations.

Pareto front analyses revealed strong constraints on the joint optimization of μ_{max} and niche-determining traits across all environmental gradients we considered (Fig. 2A-E). In each case, we found that phenotypic distributions were bounded by Pareto fronts, indicating trade-offs between maximum growth rate and competitive or tolerance traits. The area of phenotypic space excluded by these fronts significantly exceeded randomized null expectations (39) across all gradients (empty-space randomization test; μ_{max} (N) ~ $1/N^*$, $P = 0.003$; μ_{max} (S) ~ c, $P = 0.046$; μ_{max} (I, P, T) ~ $1/I^*$, $1/P^*$, T_{br}, all $P \leq 0.001$). Critically, we also found that median (50th quantile) regressions were significantly negative within individual niche axes (Figs. 2, 5A), indicating that trade-offs between μ_{max} and niche-determining traits extend broadly across phenotypic space in *C. reinhardtii*, rather than occurring only among Pareto-optimal phenotypes. Supplemental analyses corroborated the existence of Pareto fronts (quantile regressions) and significant negative trait correlations (PCA, see SI *Results*).

Pareto fronts reveal trade-offs among different niche-determining traits in *Chlamydomonas reinhardtii*. Trade-offs between growth and niche-determining traits are expected to arise from physiological constraints within individual niche axes, but relationships among traits governing performance across multiple niche axes (e.g. salt and temperature) in phytoplankton may reflect more complex genetic patterns. Antagonistic pleiotropy can generate negative correlations between traits (12, 13), but synergistic pleiotropy can improve multiple traits simultaneously, and modular or independent traits may evolve with little effect on others (21, 40). To evaluate the structure of these relationships among niche-determining traits in *C. reinhardtii*, we applied both Pareto front and quantile regression analysis to traits governing performance across different niche axes.

Pareto front analyses revealed several constraints on the simultaneous optimization of niche-determining traits across niche axes (Fig. 3). Significant Pareto fronts bounded relationships between T_{br} and $1/I^*$, T_{br} and c, and $1/N^*$ and c (empty-space randomization tests, $P = 0.014$, 0.019, and 0.027, Fig. 3DFJ). We detected additional Pareto fronts between $1/P^*$ and $1/N^*$, $1/I^*$, and c (empty-space randomization test, $P = 0.048$, 0.022, and 0.041, Fig. 3BEF). These results, however, were only significant when we restricted the analysis to phenotypes near the putative Pareto front (upper third of the data). Given that our populations were not selected to optimize traits relevant to all niche axes and the relatively short duration of our experimental evolution (51), much of the phenotypic variation we observed reflects sub-optimal trait combinations. Restricting analyses to phenotypes nearest the Pareto fronts therefore improved our statistical detection of these constraints. Notably, Pareto fronts emerged among several niche-determining traits despite positive correlations in the underlying data ($1/P^*$ with $1/I^*$ and $1/N^*$, Fig. 3BE, Fig. 5A), indicating that multivariate constraints can persist even when traits covary positively overall.

Trait covariance shapes evolutionary shifts towards Pareto-optimal trait combinations. To evaluate how experimental evolution reshaped trait variation, we tested whether populations

evolved under specific abiotic conditions disproportionately occupied Pareto-optimal regions of trait space. For each comparison of growth rate and niche-determining traits within individual niche axes (Fig. 2) and between niche-determining traits (Fig. 3), we fit secondary "inner" Pareto fronts to the 75% of observations closest to the minimal trait combinations (Figs. S10-S11). We then tested whether populations evolved under matching environmental conditions were more likely to exceed these inner fronts relative to randomized null expectations ("Pareto optimization test").

Experimental evolution produced clear, condition-specific shifts toward some Pareto-optimal trait combinations. Populations that evolved under salt stress significantly optimized the relationship between μ_{max} (S) and salt tolerance relative to ancestral and non-matching (i.e. non-salt stress evolved) populations (Pareto optimization test, $P < 0.001$, Figs. 2D, S10D), pushing evolved populations toward the Pareto front. Although we detected no other cases of evolutionary optimization associated with our selection treatments within individual niche axes (Fig. 2), experimental evolution shifted *C. reinhardtii* populations into Pareto-optimal space for the majority (7/10) of comparisons across niche axes (Figs. 3, 5B). In each case, populations evolved under matching environmental conditions disproportionately contributed to the realized Pareto front, indicating directional evolutionary movement toward constrained optima.

The extent to which evolution produced joint trait optimization was strongly predicted by the structure of trait covariance behind a Pareto front. Across relationships between μ_{max} and corresponding niche-determining traits, significant negative correlations in the underlying trait data were associated with little evidence of evolutionary movement toward Pareto-optimal trait combinations (Figs. 2, 5B). In contrast, populations frequently optimized performance across multiple niche axes when underlying trait correlations were positive ($1/P^*$ with $1/I^*$ and $1/N^*$, Fig. 3BE) or near zero (Fig. 3CGHJ).

Mixed-effects models indicated that evolutionary optimization frequently relied on indirect responses to selection. Populations evolved under phosphorus limitation, for example, showed increased competitive ability for light and nitrogen, generating positive correlations between $1/P^*$ with $1/I^*$ and $1/N^*$ that facilitated joint optimization of these traits (Table S3, Fig. 3BE). Tellingly, the primary exception to these trends involved salt tolerance, where evolutionary optimization consistently occurred in salt-adapted populations regardless of correlations with other niche-determining traits (Figs. 2D, 3CFHJ, 5B). These patterns were driven by large evolutionary increases in salt tolerance in populations that evolved under salinity stress (Table S3), changes that occurred largely independently of other niche-determining traits (Fig. 3CFHJ).

Pareto fronts reveal broad trade-offs across phytoplankton niche axes. To evaluate whether Pareto constraints observed in our experimental evolution extend across macroevolutionary scales, we compiled estimates of growth rates and niche-determining traits across light, nitrogen, phosphorus, and temperature gradients for a broad range of phytoplankton taxa. After fitting thermal performance and Monod curves and screening model fits for quality (SI Appendix), the final dataset comprised 499 observations spanning 299 species and strains. To evaluate constraint in this broader, cross-species phenotypic space, we applied both Pareto front analyses and tests for triangular trait distributions consistent with optimization across multiple ecological axes (35).

Across species, we detected strong evidence of constrained trait combinations involving growth rate and niche-determining traits. We detected significantly triangular (relative to randomized null expectations) trait distributions consistent with Pareto optimization for light and phosphorus utilization (triangularity, $P = 0.01$ and 0.003, respectively, Fig. 4AH), but not for nitrogen or thermal traits (triangularity, $P = 0.143$ and 0.181, Fig. 4EJ). Consistent with these patterns, we found that putative Pareto fronts significantly constrained the phenotypic space occupied in our μ_{max} (I) ~ $1/I^*$ and μ_{max} (P) ~ $1/P^*$ relationships (empty space randomization test, $P \leq 0.005$). We also detected evidence of Pareto fronts constraining the joint optimization of μ_{max} (T) and T_{br} (Fig. 4J) across

phytoplankton when analyses were restricted to phenotypes nearest the Pareto front (upper third data set, empty space randomization test, $P \leq 0.001$).

Pareto fronts also constrained relationships among niche-determining traits across phytoplankton species. Using species-averaged trait values, we found significant evidence of Pareto fronts that constrained simultaneous optimization of $1/I^*$ and $1/N^*$, $1/I^*$ and $1/P^*$, $1/I^*$ and T_{br}, and $1/N^*$ and T_{br} (empty space randomization test, $P = 0.002$, 0.010, 0.005, and 0.001, Fig. 4BCDG). We detected significantly triangular constraint envelopes for only a subset of these relationships ($1/N^*$ with $1/I^*$ and T_{br}; triangularity, $P = 0.027$ and 0.032, Fig. 4BG). In most cases these constraints were only evident after the exclusion of a single extreme outlier species with exceptionally (>90th quantile) high performance along both niche axes (Fig. 4), which we excluded to evaluate broader patterns of constraint across phytoplankton.

Micro- and macroevolutionary trade-offs differ across phytoplankton. The patterns we observed in experimentally evolved populations of *Chlamydomonas reinhardtii* did not always extend to macroevolutionary relationships among phytoplankton species. Among our *C. reinhardtii* populations, we observed consistently negative trait correlations between μ_{max} and niche-determining traits within individual niche axes (Fig. 2). However, negative correlations were not evident across diverse phytoplankton taxa (Figs., S13-S14, Table S4). Despite the absence of these negative correlations at the macroevolutionary scale, we detected strong evidence of Pareto fronts constraining the joint optimization of μ_{max} and niche-determining traits within light, phosphorus, and temperature gradients across species (empty space randomization test, $P \leq 0.001$, Fig. 4AHJ). These constraints closely mirrored those observed in experimental *C. reinhardtii* populations (empty space randomization test, $P \leq 0.005$, Figs. 2ABCE, 5C), suggesting that while evolutionary diversification and innovation can relax and overcome trait correlations, underlying physiological limits on growth and resource use optimization persist across phytoplankton.

In contrast to comparisons within niche axes, relationships between niche-determining traits across niche axes were rarely consistent across evolutionary scales. For several relationships, we detected Pareto fronts only at one evolutionary scale (Fig. 5C). Among experimentally evolved populations, we detected a significant Pareto front between $1/N^*$ and $1/P^*$ (empty space randomization test, $P = 0.048$; Fig. 3E) that was absent in our cross-species analysis. Conversely, significant Pareto fronts between $1/N^*$ and both $1/I^*$ and T_{br} were detected across phytoplankton species (empty space randomization test, $P \leq 0.005$, Fig. 4BG) but were not observed within our experimentally evolved populations (Fig. 5C). We did however find consistent evidence for Pareto constraints across micro- and macroevolutionary scales in 2 of 6 relationships ($1/I^*$ and $1/P^*$ and $1/I^*$ and T_{br}, empty space randomization test, $P \leq 0.025$, Fig. 5C).

Discussion

In this study, we demonstrate widespread Pareto fronts constraining relationships between growth rates and key niche-determining traits—including thermal breadth, competitive abilities for resources, and salt tolerance—in phytoplankton. These constraints are evident at both microevolutionary scales, within experimentally evolved populations of *Chlamydomonas reinhardtii*, and macroevolutionary scales, across 299 phytoplankton taxa, highlighting the central role of trade-offs in shaping phenotypic evolution. Critically, such trade-offs do not necessarily manifest as simple negative correlations among traits (3, 5, 21) but instead emerge most clearly among Pareto-optimal genotypes. By defining the upper bounds of performance, Pareto fronts delineate regions of phenotypic space that are effectively inaccessible, explaining the persistent absence of large portions of theoretically possible phenotypic space across the tree of life (35, 39, 40).

Within phytoplankton communities, trade-offs among traits associated with nutrient acquisition and utilization, growth, and cell morphology are widely implicated in driving ecological divergence and maintaining biodiversity (23). Here, we find strong evidence for trade-offs between niche-

determining traits and maximum growth rates that recapitulate classic gleaner-opportunist trade-offs in nutrient acquisition (20–22), generalist-specialist trade-offs in thermal traits (26), and salt tolerance-growth trade-offs (24, 25). In our study, these trade-offs—manifesting as negative correlations between traits—consistently emerged among experimentally evolved *C. reinhardtii* populations (Fig. 5A, Table S1). This pattern suggests that ecological trade-offs in phytoplankton can arise from direct evolutionary constraints such as antagonistic pleiotropy or resource allocation trade-offs (13, 23, 47) generating negative trait correlations that are not readily overcome through short-term adaptive evolution.

Despite their central role in ecology and evolution (4, 8, 11, 23, 27, 29, 42, 44), trade-offs can often be difficult to detect empirically, even for traits expected to incur substantial costs (31–33). When organisms differ widely in overall quality or resource budgets, positive correlations can obscure trade-offs that manifest only among relatively optimized genotypes. By explicitly testing whether phenotypic distributions were bounded by Pareto fronts, our evolution experiments revealed constraints on the joint optimization of niche-determining traits in *Chlamydomonas reinhardtii* (Fig. 3). For example, we detected strong Pareto constraints on the joint optimization of competitive abilities for phosphorus with light and nitrogen despite significant positive correlations between these traits (Fig. 5A). These results help reconcile observations of convergent evolution towards increased competitiveness for multiple essential nutrients (21, 30) with theoretical and empirical explorations of the importance of trade-offs in structuring communities (11, 23). Behind Pareto fronts that define intractable limits to multivariate trait optimization, adaptive evolution can generate positive correlations between traits, illustrating how evolutionary constraints on organismal performance can persist concurrently with adaptive trait correlations (3) (Fig. 5A).

In our experimentally evolved *C. reinhardtii* populations, genotypes were only able to optimize multiple niche-determining traits simultaneously when the underlying correlation between traits were neutral (e.g. $1/N^*$ v. T_{br}) or positive (Fig. 5B); negative correlations were instead associated with limited movement towards Pareto optimality. These patterns suggest that the structure of multivariate genetic covariance behind a Pareto front strongly influences whether evolution can approach an optimal trade-off surface or remains constrained by genetic architecture prior to reaching it (13, 39, 40). We suggest that the patterns we observe here are consistent with evolutionary trajectories under rapidly changing or fluctuating environments, where mutations with large, positively pleiotropic effects are initially favored before populations approach ultimate performance limits. As populations move closer to these limits, selection may increasingly favor modular mutations of smaller effect, revealing negative correlations among optimized genotypes under relatively stable conditions (40, 51, 53–55). Evolution toward Pareto-optimal trait combinations may also occur through large shifts in comparatively modular or independent traits. In our experiment, salt tolerance evolved consistently under salinity stress without detectable antagonistic effects on other niche-determining traits, allowing populations to approach Pareto fronts across multiple niche axes (Fig. 5B).

Strikingly, several patterns observed in our experimentally evolved *Chlamydomonas reinhardtii* populations did not translate directly to macroevolutionary patterns across phytoplankton species. In particular, the negative correlations between growth rate and niche-determining traits that were pervasive within individual niche axes at the microevolutionary scale (Fig. 2) were absent across diverse phytoplankton taxa (Fig. 4). Nonetheless, we found strong evidence that performance within these niche axes remains bounded by Pareto fronts at both evolutionary scales. Across 299 phytoplankton taxa, Pareto fronts significantly constrained the joint optimization of growth rate and niche-determining traits under light and phosphorus limitation and across thermal gradients, closely mirroring the boundaries observed in experimentally evolved *C. reinhardtii* populations (Fig. 5C). The persistence of these hard limits on performance, despite the relaxation of genetic constraints over macroevolutionary timescales (47–50) and ample opportunity for evolutionary innovation suggests that some trade-offs reflect fundamental physiological or ecological limitations rather than transient genetic constraints.

Relationships among niche-determining traits across niche axes were even less consistent between micro- and macroevolutionary scales. Several trait combinations that were constrained within experimentally evolved *Chlamydomonas reinhardtii* populations did not exhibit comparable patterns across phytoplankton species, while others appeared constrained only at the macroevolutionary scale (Fig. 5C). These discrepancies likely reflect the fundamentally different evolutionary processes operating across timescales: while experimental evolution captures short-term responses within a shared genetic and physiological background, macroevolutionary patterns emerge through long-term diversification across lineages occupying distinct ecological niches (5). Over deep evolutionary time, major innovations in phytoplankton biology—including coloniality and mixotrophy—may alter or relax the genetic and physiological constraints that shape trait relationships within populations. Evidence of triangular trait distributions at the macroevolutionary scale (Fig. 4ABGH), which emerge when organisms face multivariate optimization challenges involving more than two traits (10, 25, 35), further suggests that divergence along additional trait axes contributes to these patterns. In phytoplankton, improvements in competitive ability for limiting nutrients may incur costs in other key traits such as cell size (27), defence (28), or thermal flexibility (41, 56), positioning macroevolutionary variation in such traits as a plausible mechanism for maintaining sub-optimal variation in niche-determining traits (Fig. 1D). Consistent with this interpretation, our experimental evolution data revealed Pareto fronts constraining relationships between niche-determining traits and cell size in *C. reinhardtii* (Fig. S7), hinting at three (or more)-way trade-offs capable of generating and maintaining triangular patterns of phenotypic variation across evolutionary scales.

The trade-offs we observed reflect the imprint of past adaptation to define species' ecological niches (12, 39, 40), but they will also shape—and constrain—evolutionary responses to novel and rapidly shifting selective regimes (6, 57). In this context, the Pareto fronts identified here are likely to have important consequences for how phytoplankton respond to the multivariate stressors imposed by global change, including warming, salinization, and alterations to nutrient regimes. When multiple stressors act simultaneously, trade-offs among niche-determining traits can exacerbate fitness costs by limiting the extent to which populations can optimize performance across all relevant dimensions (14–16). At the same time, correlated evolution among certain traits may facilitate adaptive responses in some contexts before populations encounter ultimately intractable limits on multivariate optimization (Figs. 1B, 5B, 12, 39, 40). Our results indicate that such limits are not merely theoretical: we detected widespread Pareto fronts constraining the joint optimization of niche-determining traits in experimentally evolved *C. reinhardtii* populations (Figs. 2–3) and comparable multivariate boundaries across phytoplankton taxa (Figs. 4, 5C). Together, these findings suggest that both adaptive evolution within species and community turnover across species in response to anthropogenic stressors occur within persistent performance boundaries. Understanding and predicting biological responses to global change therefore requires explicitly accounting for these limits on multivariate trait optimization rather than treating responses to individual stressors in isolation.

In this study, we demonstrate that widespread Pareto fronts—trade-offs that emerge among optimized genotypes—constrain the evolution of niche-determining traits across both micro- and macroevolutionary scales in phytoplankton. By extending Pareto fronts as an analytical framework for detecting context-dependent and otherwise elusive trade-offs (3, 5, 31), our results highlight their utility for understanding phenotypic evolution under constraint at multiple evolutionary timescales. Across experimental evolution and phylogenetic comparisons, we show that adaptation is not solely limited by genetic variation or opportunity, but by fundamental, multivariate limits on trait optimization. Recognizing and characterizing these limits is therefore essential for understanding how phenotypic diversity is generated, maintained, and constrained in a changing world.

Materials and Methods

Experimental evolution of *Chlamydomonas reinhardtii*. We used experimentally evolved populations of *Chlamydomonas reinhardtii* (21, 30) to examine phenotypic trade-offs among niche-determining traits. In brief, we inoculated experimental chemostats with *C. reinhardtii* cells cultured from one of four ancestral isoclonal colonies and from a genetically diverse original population. Each ancestral population was evolved under conditions of salt stress (S), light- (L), phosphorus- (P), and nitrogen- (N) limitation, and in biotically depleted media (B), a biotic depletion x salt stress interactive treatment (BS), and a control COMBO (58) treatment (C). We experimentally evolved *C. reinhardtii* populations for 285 days, after which we isolated a total of 32 descendant populations. We then used four independent replicates from each population in batch-culture experiments to assess their niche-determining traits (competitive abilities for light ($1/I^*$), nitrogen ($1/N^*$), and phosphorus ($1/P^*$) as well as salt tolerance (c) and thermal breadth (T_{br}). Full details on the design and implementation of our experimental evolution are available in the SI Supporting Materials and Methods.

Growth assays and estimation of niche-determining traits. We quantified *Chlamydomonas reinhardtii* growth across gradients of light, nitrogen, phosphorus, salinity, and temperature, generating high-resolution growth time series. We fit growth data with thermal performance curves, Monod functions, and inverse logistic growth models to estimate niche-determining traits (Fig. S1), including maximum growth rate (μ_{max}), competitive abilities for light, nitrogen, and phosphorus ($1/R^*$), salt tolerance (c), and thermal breadth (Tbr). Full details of experimental design, model selection, and fitting procedures are provided in the SI Supporting Materials and Methods.

Detection and statistical evaluation of Pareto fronts. To identify trade-offs constraining multivariate trait optimization, we analyzed bivariate relationships among niche-determining traits to detect putative Pareto fronts — upper boundaries of phenotypic covariation beyond which simultaneous optimization of multiple traits is not observed (39, 40). We estimated Pareto fronts using convex hull algorithms, and we quantified the area of phenotypic space rendered inaccessible by these fronts. We assessed the statistical significance of Pareto fronts using an empty space randomization test in which we compared the size of observed inaccessible space to null distributions generated by randomization of trait values (39).

We complemented this approach with quantile regression analyses, which test for negative relationships at the upper bounds of trait distributions and thus capture trade-offs among optimized phenotypes even when overall correlations may be positive (3). Additionally, we used fitted 50th quantile regressions to assess general patterns of trait covariation. Because our data included a high proportion of sub-optimal trait combinations located far behind a putative Pareto front that reduced our statistical power to interrogate relationships among Pareto-optimal phenotypes, we conducted all analyses on both the full dataset and a trimmed dataset restricted to the upper third of phenotypes based on scaled Euclidean distance from minimal (x, y) values. Additional methodological details are provided in the SI Supporting Materials and Methods.

To test whether experimental evolution resulted in the optimization of combinations of traits corresponding to the evolutionary environment (e.g. evolution of increased maximum growth rate or salt tolerance under salt stress), we fit a secondary Pareto front to the 75% of our data closest to the minimal (x,y) values based on scaled Euclidean distance for all trait comparisons (which we term the “inner Pareto front”). By comparing the location of trait combinations from populations that evolved under corresponding evolutionary conditions (e.g. $1/N^*$ values of replicates from nitrogen-limited populations), we were able to quantify the likelihood that populations evolved in a given environment improved traits associated with fitness in that environment (e.g. higher salt tolerance in a high salt environment), and whether these improvements led to Pareto-optimal trait combinations. To test the significance of evolutionary shifts in trait values towards Pareto-optimal solutions, we compared the number of observations for matching replicates above this 75th quantile to those generated from simulated null data.

Synthesis and analysis of phytoplankton trait variation across species. To assess whether constraints observed in experimental evolution in single species extend across broader macroevolutionary scales, we compiled published estimates of phytoplankton growth rates measured across gradients of light, nitrogen, phosphorus, and temperature. We synthesized estimates of phytoplankton growth rates across these gradients and estimated niche-determining trait values. After performing quality controls on our fitted models, we were left with 499 resource or temperature - dependent growth models for 299 phytoplankton strains and species. We then analyzed bivariate trait relationships across species using convex hull – based Pareto front methods and null randomizations to quantify inaccessible phenotypic space. To test for multivariate optimization across more than two traits (35), we additionally assessed triangular patterns of trait variation following established methods for detecting task specialization and archetypes. Full details on data compilation, model fitting, and statistical analyses are provided in the SI Supporting Materials and Methods.

Data, materials, and software availability. All code and data required to replicate analyses and generate figures are archived at Zenodo (https://zenodo.org/records/19112865, DOI: 10.5281/zenodo.19112865) and available via GitHub (https://github.com/JasonLaurich/Chlamy_37_pops_pheno_constraint).

Acknowledgments. We thank Daniel Steiner for assistance with HPLC analysis, Ken Thompson for manuscript feedback, and Megan Szojka for code review. Our work was supported by a Natural Sciences and Engineering Research Council of Canada (NSERC) Discovery Grant and a Canada First Research Excellence Fund Grant awarded to J.R.B. J.R.B.'s work during the experimental phase of this study was supported by a Nippon Foundation Nereus Postdoctoral Fellowship. We also thank members of the Bernhardt Lab for helpful feedback on an earlier version of this manuscript.

References

1. C. Darwin, *On the origin of species by means of natural selection or the preservation of Favored Races in the Struggle for Life*, 1998th Ed. (Modern Library, 1859).
2. A. A. Agrawal, J. K. Conner, S. Rasmann, "Tradeoffs and negative correlations in evolutionary ecology" in *Evolution after Darwin: The First 150 Years*, (Sinauer Associates, 2010), pp. 243–268.
3. M. T. J. Johnson, Z. Nassrullah, The improbability of detecting trade-offs and some practical solutions. *J. Evol. Biol.* **37**, 1205–1214 (2024).
4. T. Garland, C. J. Downs, A. R. Ives, Trade-offs (and constraints) in organismal biology. *Physiol. Biochem. Zool.* **95**, 82–112 (2022).
5. A. A. Agrawal, A scale-dependent framework for trade-offs, syndromes, and specialization in organismal biology. *Ecology* **101**, e02924 (2020).
6. R. Law, Optimal life histories under age-specific predation. *Am. Nat.* **114**, 399–417 (1979).
7. J. Antonovics, The input from population genetics: "the new ecological genetics." *Syst. Bot.* **1**, 233–245 (1976).
8. E. Ehrlich, N. J. Kath, U. Gaedke, The shape of a defense-growth trade-off governs seasonal trait dynamics in natural phytoplankton. *ISME J.* **14**, 1451–1462 (2020).
9. A. Posfai, T. Taillefumier, N. S. Wingreen, Metabolic trade-offs promote diversity in a model ecosystem. *Phys. Rev. Lett.* **118**, 028103 (2017).
10. D. J. Futuyma, G. Moreno, The evolution of ecological specialization. *Annu. Rev. Ecol. Syst.* **19**, 207–233 (1988).

11. D. Tilman, *Resource competition and community structure* (Princeton University Press, 1982).
12. R. Lande, Quantitative genetic analysis of multivariate evolution, applied to brain: body size allometry. *Evolution* **33**, 402–416 (1979).
13. R. Lande, S. J. Arnold, The measurement of selection on correlated characters. *Evolution* **37**, 1210–1226 (1983).
14. H. R. P. Phillips, *et al.*, Global changes and their environmental stressors have a significant impact on soil biodiversity—a meta-analysis. *iScience* **27**, 110540 (2024).
15. N. Hu, P. E. Bourdeau, J. Hollander, Responses of marine trophic levels to the combined effects of ocean acidification and warming. *Nat. Commun.* **15**, 3400 (2024).
16. T. Wang, *et al.*, Interactions between climate warming, herbicides, and eutrophication in the aquatic food web. *J. Environ. Manage.* **345**, 118753 (2023).
17. D. B. V. de Van de Waal, E. Litchman, Multiple global change stressor effects on phytoplankton nutrient acquisition in a future ocean. *Philos. Trans. R. Soc. B* (2020). https://doi.org/10.1098/rstb.2019.0706.
18. C. B. Field, M. J. Behrenfeld, J. T. Randerson, P. Falkowski, Primary production of the biosphere: integrating terrestrial and oceanic components. *Science* **281**, 237–240 (1998).
19. P. G. Falkowski, R. T. Barber, V. Smetacek, Biogeochemical controls and feedbacks on ocean primary production. *Science* **281**, 200–206 (1998).
20. J. P. Grover, Resource competition in a variable environment: phytoplankton growing according to Monod's model. *Am. Nat.* **136**, 771–789 (1990).
21. J. R. Bernhardt, *et al.*, The evolution of competitive ability for essential resources. *Philos. Trans. R. Soc. B Biol. Sci.* **375**, 20190247 (2020).
22. K. F. Edwards, C. A. Klausmeier, E. Litchman, A three-way trade-off maintains functional diversity under variable resource supply. *Am. Nat.* **182**, 786–800 (2013).
23. E. Litchman, C. A. Klausmeier, O. M. Schofield, P. G. Falkowski, The role of functional traits and trade-offs in structuring phytoplankton communities: scaling from cellular to ecosystem level. *Ecol. Lett.* **10**, 1170–1181 (2007).
24. J. P. Grime, Evidence for the existence of three primary strategies in plants and Its relevance to ecological and evolutionary theory. *Am. Nat.* **111**, 1169–1194 (1977).
25. T. J. Flowers, P. F. Troke, A. R. Yeo, The mechanism of salt tolerance in halophytes. *Annu. Rev. Plant Physiol.* **28**, 89–121 (1977).
26. R. B. Huey, J. G. Kingsolver, Evolution of thermal sensitivity of ectotherm performance. *Trends Ecol. Evol.* **4**, 131–135 (1989).
27. K. F. Edwards, C. A. Klausmeier, E. Litchman, Evidence for a three-way trade-off between nitrogen and phosphorus competitive abilities and cell size in phytoplankton. *Ecology* **92**, 2085–2095 (2011).
28. T. Réveillon, L. Becks, Trade-offs between defense and competitive traits in a planktonic predator–prey system. *Ecology* **105**, e4456 (2024).
29. R. M. S. Saggere, C. W. J. Lee, I. C. W. Chan, D. G. Durnford, A. M. Nedelcu, A life-history trade-off gene with antagonistic pleiotropic effects on reproduction and survival in limiting environments. *Proc. R. Soc. B Biol. Sci.* **289**, 20212669 (2022).
30. M. Tamminen, *et al.*, Proteome evolution under non-substitutable resource limitation. *Nat. Commun.* **9**, 4650 (2018).

31. C. Chang, M. Moiron, A. Sánchez-Tójar, P. T. Niemelä, K. L. Laskowski, What is the meta-analytic evidence for life-history trade-offs at the genetic level? *Ecol. Lett.* **27**, e14354 (2024).
32. F. Douhard, *et al.*, How much energetic trade-offs limit selection? Insights from livestock and related laboratory model species. *Evol. Appl.* **14**, 2726–2749 (2021).
33. A. J. Van Noordwijk, G. de Jong, Acquisition and allocation of resources: their influence on variation in life history tactics. *Am. Nat.* **128**, 137–142 (1986).
34. D. Reznick, L. Nunney, A. Tessier, Big houses, big cars, superfleas and the costs of reproduction. *Trends Ecol. Evol.* **15**, 421–425 (2000).
35. O. Shoval, *et al.*, Evolutionary trade-offs, pareto optimality, and the geometry of phenotype space. *Science* **336**, 1157–1160 (2012).
36. L. Bliard, *et al.*, Detecting context dependence in the expression of life history trade-offs. *J. Anim. Ecol.* **94**, 379–393 (2025).
37. C. Yang, *et al.*, Carbon resource richness shapes bacterial competitive interactions by alleviating growth-antibiosis trade-off. *Funct. Ecol.* **33**, 868–875 (2019).
38. E. G. King, D. A. Roff, D. J. Fairbairn, Trade-off acquisition and allocation in *Gryllus firmus*: a test of the Y model. *J. Evol. Biol.* **24**, 256–264 (2011).
39. Y. Li, D. A. Petrov, G. Sherlock, Single nucleotide mapping of trait space reveals Pareto fronts that constrain adaptation. *Nat. Ecol. Evol.* **3**, 1539–1551 (2019).
40. G. Kinsler, Y. Li, G. Sherlock, D. A. Petrov, A high-resolution two-step evolution experiment in yeast reveals a shift from pleiotropic to modular adaptation. *PLOS Biol.* **22**, e3002848 (2024).
41. A. L. Heinrichs, M. Gerhard, M. Striebel, Interactive effects of light and nutrients shape phytoplankton thermal traits. *Sci. Rep.* **15**, 40345 (2025).
42. M. Zaret, L. Kinkel, E. T. Borer, E. W. Seabloom, Plant growth–defense trade-offs are general across interactions with fungal, insect, and mammalian consumers. *Ecology* **105**, e4290 (2024).
43. I. J. Wright, *et al.*, The worldwide leaf economics spectrum. *Nature* **428**, 821–827 (2004).
44. E. M. Lind, *et al.*, Life-history constraints in grassland plant species: a growth-defence trade-off is the norm. *Ecol. Lett.* **16**, 513–521 (2013).
45. Z. Wen, *et al.*, Tradeoffs among root morphology, exudation and mycorrhizal symbioses for phosphorus-acquisition strategies of 16 crop species. *New Phytol.* **223**, 882–895 (2019).
46. R. W. Heckman, F. W. Halliday, C. E. Mitchell, A growth–defense trade-off is general across native and exotic grasses. *Oecologia* **191**, 609–620 (2019).
47. D. Schluter, Adaptive radiation along genetic lines of least resistance. *Evolution* **50**, 1766–1774 (1996).
48. J. Costa e Silva, B. M. Potts, P. A. Harrison, Population divergence along a genetic line of least resistance in the tree species *Eucalyptus globulus*. *Genes* **11**, 1095 (2020).
49. J. W. McGlothlin, *et al.*, Adaptive radiation along a deeply conserved genetic line of least resistance in *Anolis* lizards. *Evol. Lett.* **2**, 310–322 (2018).
50. L. A. Donovan, H. Maherali, C. M. Caruso, H. Huber, H. de Kroon, The evolution of the worldwide leaf economics spectrum. *Trends Ecol. Evol.* **26**, 88–95 (2011).
51. M. J. Wiser, N. Ribeck, R. E. Lenski, Long-term dynamics of adaptation in asexual populations. *Science* **342**, 1364–1367 (2013).
52. V. Klee, M. C. Laskowski, Finding the smallest triangles containing a given convex polygon. *J. Algorithms* **6**, 359–375 (1985).

53. S. Venkataram, *et al.*, Development of a comprehensive genotype-to-fitness map of adaptation-driving mutations in yeast. *Cell* **166**, 1585-1596.e22 (2016).
54. R. Kassen, The experimental evolution of specialists, generalists, and the maintenance of diversity. *J. Evol. Biol.* **15**, 173–190 (2002).
55. M. S. Johnson, *et al.*, Phenotypic and molecular evolution across 10,000 generations in laboratory budding yeast populations. *eLife* **10**, e63910 (2021).
56. S. Levasseur, *et al.*, Warm-loving species perform well under limiting resources: trait combinations for future climate. *Glob. Change Biol.* **31**, e70554 (2025).
57. N. B. Metcalfe, How can we best measure the energetic trade-offs faced by animals? *J. Exp. Biol.* **228**, jeb250303 (2025).
58. S. S. Kilham, D. A. Kreeger, S. G. Lynn, C. E. Goulden, L. Herrera, COMBO: a defined freshwater culture medium for algae and zooplankton. *Hydrobiologia* **377**, 147–159 (1998).

612 **Figures and Tables**
613

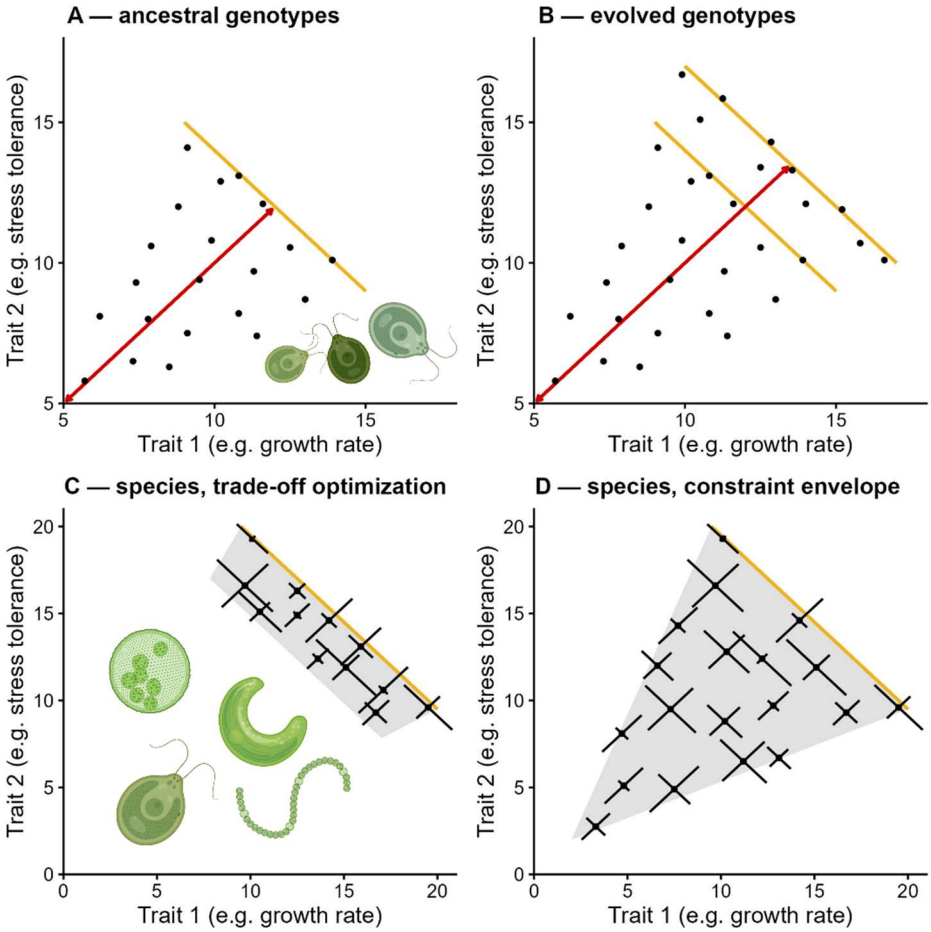

614

615 **Figure 1.** Schematic representation of sources and configuration of trade-offs and their effects on
616 phenotypic variation. (A) Among genotypes, trait correlations can be positive (red arrow) when
617 variation in individual quality (33) is larger than variation along a trade-off axis. Nonetheless,
618 negative correlations should appear among optimized genotypes, in the form of a Pareto front (3)
619 (yellow line). (B) When populations are exposed to novel conditions that impose strong selection
620 on the optimization of trait sets, evolutionary responses may escape the historical Pareto front to
621 establish a new one. (C) When traits are under strong selection for co-optimization across
622 macroevolutionary time, species should sort themselves tightly along an optimized Pareto front
623 dictating trait co-variation. (D) Constraint envelope mapping multivariate trait variation across
624 species. When the optimization of a particular trade-off is at odds with other aspects of fitness or
625 there is only weak selection for maximizing a set of traits in a trade-off, phenotypic variation among
626 species will manifest as triangular distributions, where each vertex represents a distinct archetype
627 with optimal trait combinations for a particular task or strategy (35).

628

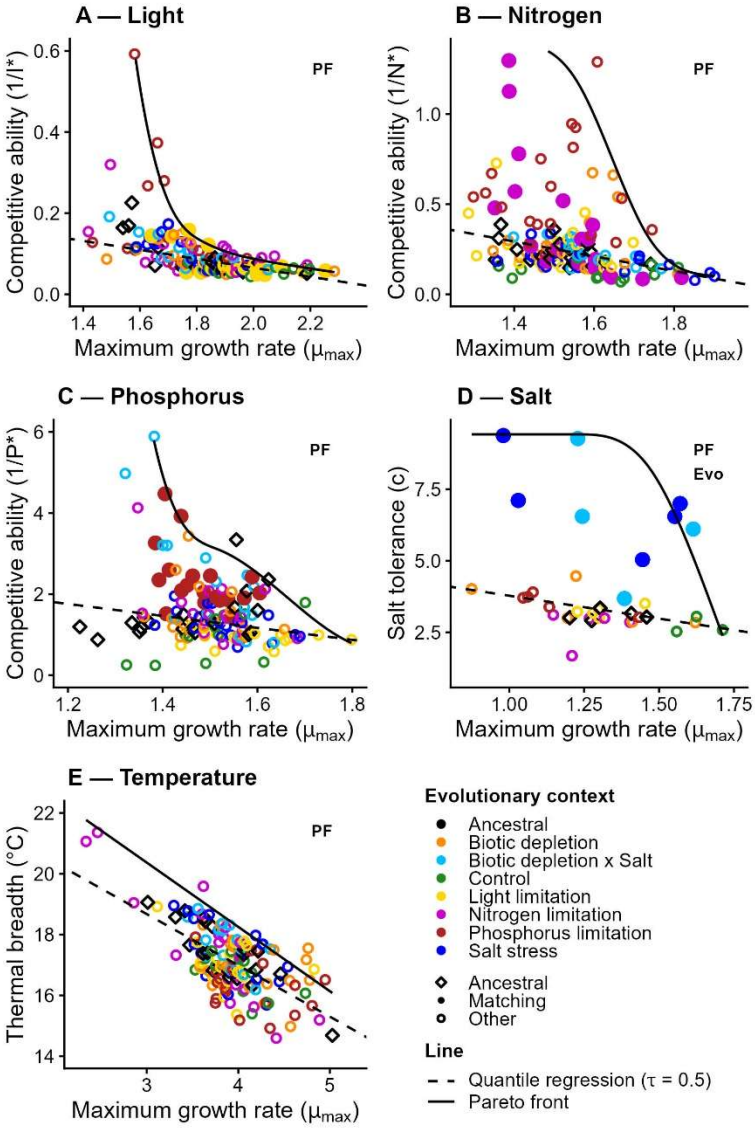

Figure 2. Tradeoffs between maximum exponential growth rate (μ_{max}) and niche-determining traits in experimentally evolved *Chlamydomonas reinhardtii* populations. (A-C) Tradeoffs between nutrient competitive abilities ($1/R^*$) and μ_{max} for light, nitrogen, and phosphorus limitation. (D) Tradeoff between salt tolerance (c) and μ_{max}. (E) Tradeoff between thermal breadth (T_{br}) and μ_{max}. Trait data for populations that evolved under the corresponding selective environment(s) (e.g. under light limitation in (A)) are represented by larger filled circles, while smaller open circles represent populations experimentally evolved under non-matching selective environments. Pareto fronts fit with shape-constrained additive models are plotted for the set of Pareto-optimal points (solid lines). Trait correlations are plotted as 50th quantile regressions (dashed lines). Significant Pareto fronts (which result in more empty space in the upper right of plots than expected under random chance) and significant 50th quantile regressions are plotted in black. Text labels in the upper right provide further information on the results of statistical testing (PF: a significant Pareto front exists and constrains phenotypic variation, Evo: experimental evolution has shifted replicates towards Pareto-optimal trait combinations). We determined whether experimental evolution increased the value of relevant traits in matching populations (Evo) by quantifying whether trait values for matching populations exceeded inner Pareto fronts (fit on trait data whose values fall within the 75th quantile distribution) more often than expected by chance alone (see Fig. S10).

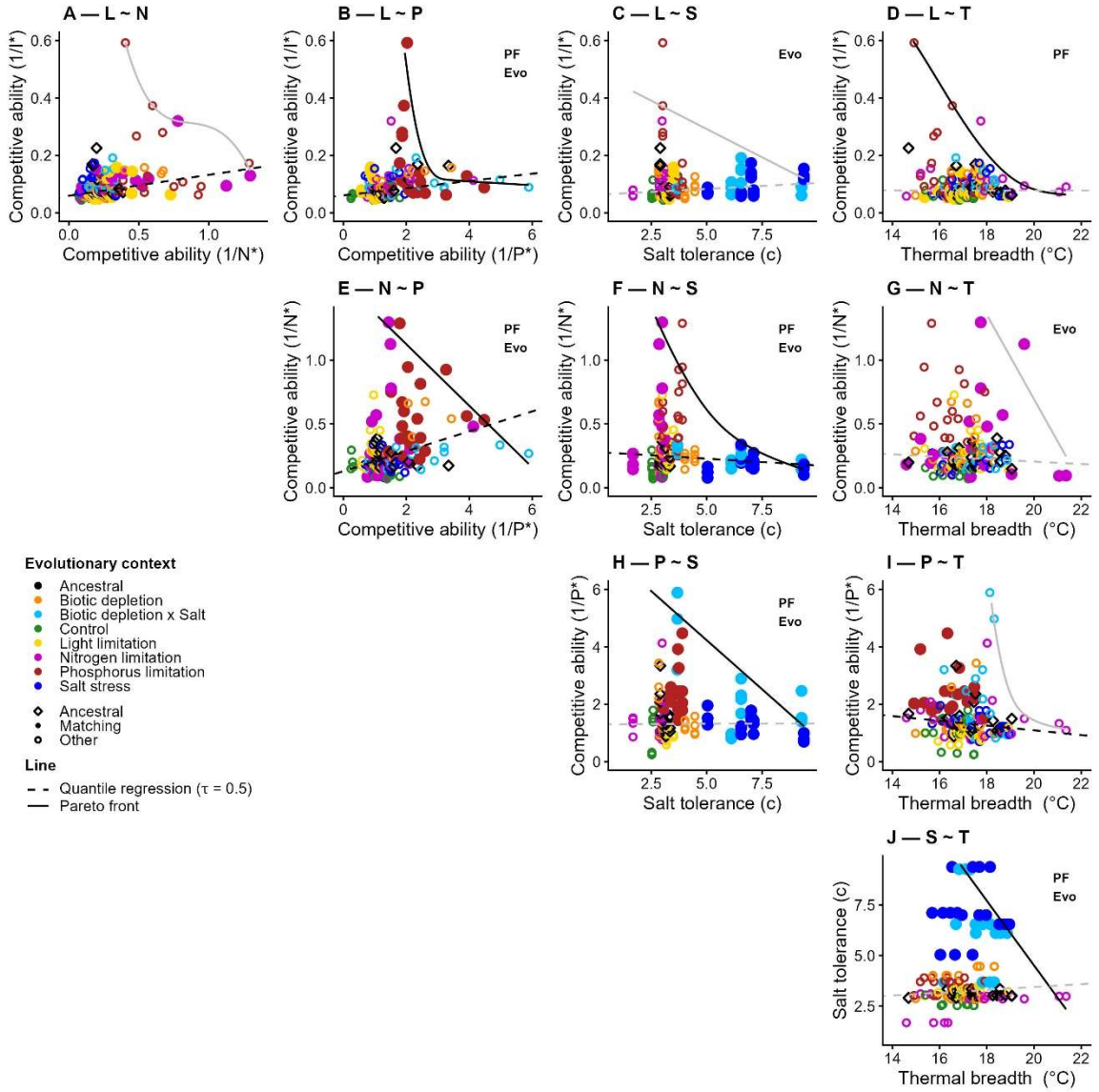

Figure 3. (A-J) Tradeoffs between nutrient competitive abilities (1/*R**) for light (L), nitrogen (N), and phosphorus (P), thermal breadth (T, T_{br}) and salt (S) tolerance in experimentally evolved and ancestral *Chlamydomonas reinhardtii* populations. Niche-determining traits are plotted in a single row and/or column. In all plots, smaller empty circles represent the traits of populations that experimentally evolved under conditions not matching either niche axis, while larger filled circles represent populations whose evolutionary history match either relevant niche-determining trait. For all relationships, we plot Pareto fronts fit to Pareto-optimal points using shape-constrained additive models (solid lines), and the 50th quantile regressions (dashed lines) to assess trait correlations. Significant Pareto fronts (that restrict bivariate phenotypic optimization more than expected by chance alone) and quantile regressions are plotted in black, while non-significant relationships are shown in grey. Additional information on statistical testing is communicated through text labels in the upper right of panels (PF: a significant Pareto front exists and constrains phenotypic variation, Evo: experimental evolution has shifted populations towards Pareto-optimal trait combinations).

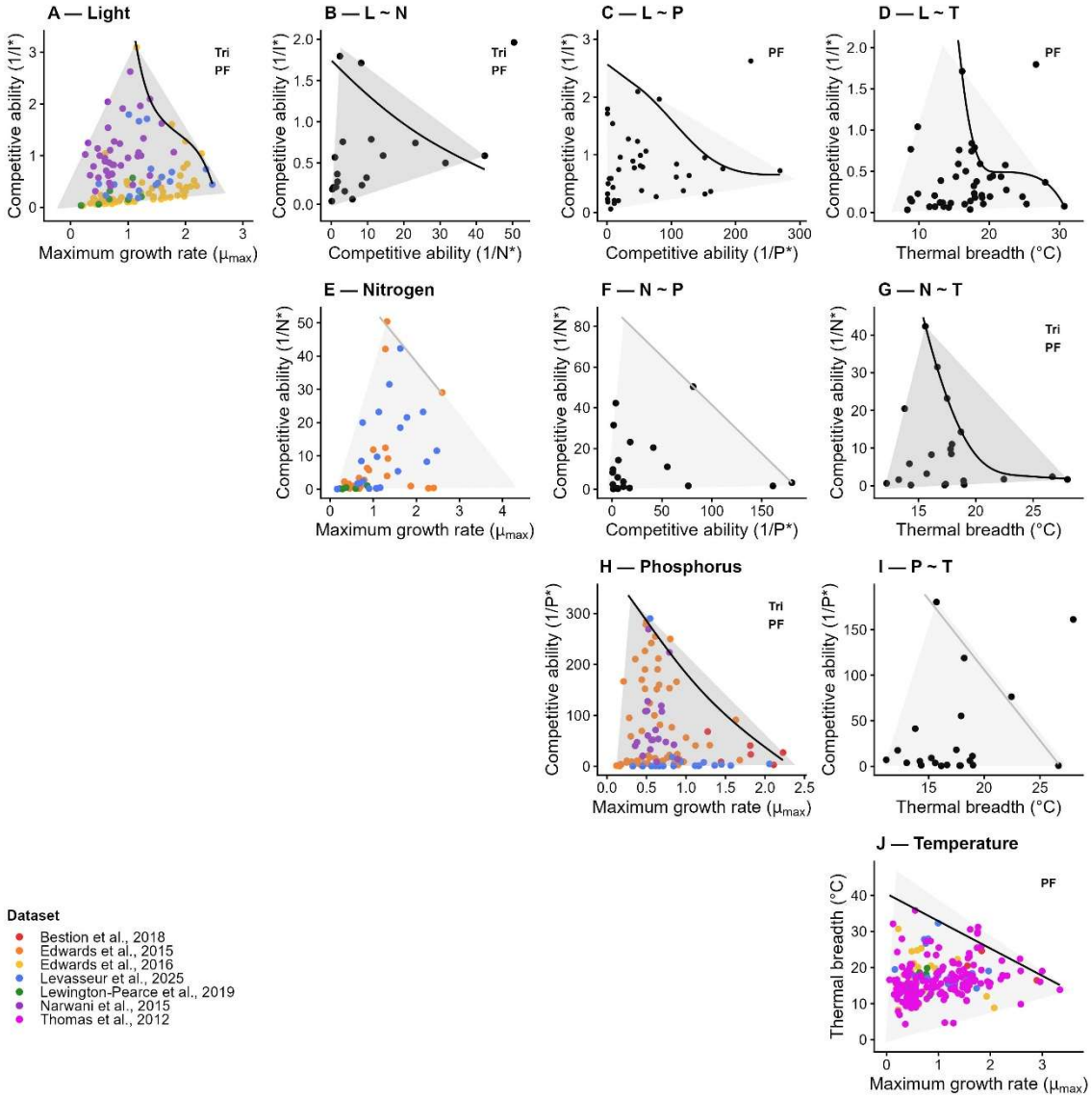

Figure 4. Tradeoffs between maximum exponential growth rate (μ_{max}), competitive abilities for nutrients ($1/R^*$) for light (L), nitrogen (N), and phosphorus (P), and thermal breadth (T, T_{br}) for a broad swath of phytoplankton species. Plots on the diagonals (A, E, H, J) were fit to the full synthesis data sets, whereas plots off the diagonals (B-D, F-G, I) represent trait values averaged for each unique species present in the synthesized data. Solid lines represent the location of Pareto fronts fit in bivariate phenotypic space. Shaded areas are triangular suites of variation that capture the smallest triangles that fully enclose a convex hull polygon containing the underlying data. Text labels in the upper right represent the results of statistical testing. In addition to determining whether Pareto fronts constrained species' abilities to optimize both traits under consideration (PF), we also used null distributions of data to test whether observed patterns of phenotypic variation were more triangular than expected under random chance (35, 52) (Tri) due to broad constraints on multivariate trait optimization at the macroevolutionary scale. Significantly triangular relationships are also here represented through highly shaded triangles, where non-significant results are lighter. Significant Pareto fronts are represented by black lines, while non-significant Pareto fronts are shaded grey.

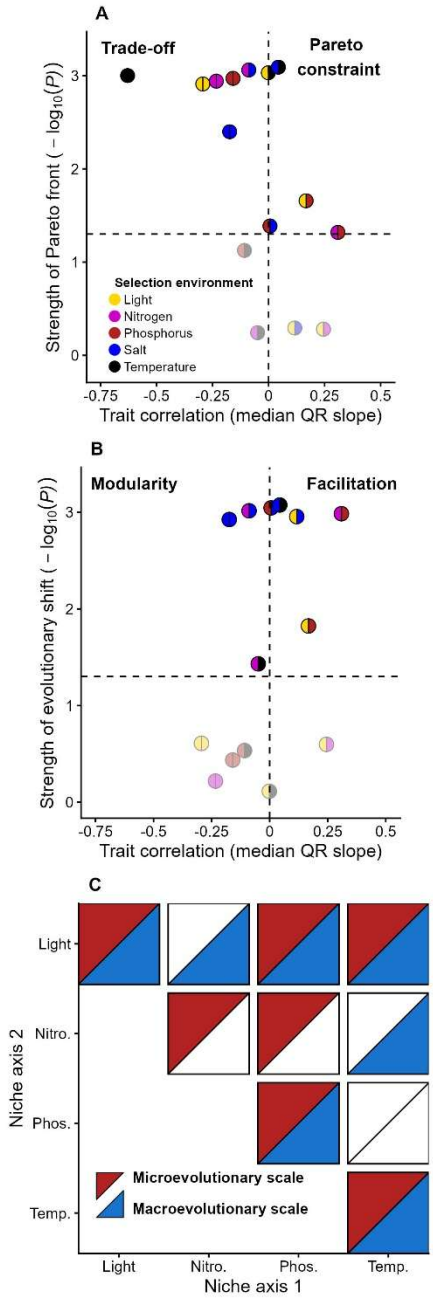

Figure 5. Summary of key results. (A) Relationship between the likelihood of observing Pareto fronts and trait correlations (median quantile regression slope). (B) Relationship between the likelihood of evolutionary optimization under relevant selection environments and trait correlations. Points correspond to trait pairs (see Figs. 2–3) and are coloured by selection environment (light, nitrogen, phosphorus, salt, temperature). Solid circles indicate relationships within a single niche axis (μ_{max} vs. niche-determining trait), whereas split circles indicate relationships across niche axes. Significant Pareto fronts or evolutionary change ($P \leq 0.05$) are shown in full colour; non-significant relationships are transparent. (C) Comparison of the occurrence of Pareto constraints across microevolutionary (experimentally evolved *Chlamydomonas reinhardtii*) and macroevolutionary (phytoplankton synthesis) scales. Filled triangles indicate whether a significant Pareto front is detected for each trait pair in each dataset.